

# Non-stoichiometry, Structure, and Properties of BiFeO<sub>3</sub> Films

Liv R. Dedon<sup>1,2</sup>, Sahar Saremi<sup>1</sup>, Zuhuang Chen<sup>1</sup>, Anoop R. Damodaran<sup>1</sup>, Brent A. Apgar<sup>1</sup>, Ran Gao<sup>1</sup>, Lane W. Martin<sup>1,2\*</sup>

<sup>1</sup> Department of Materials Science and Engineering, University of California, Berkeley, Berkeley, CA 94720, USA

<sup>2</sup> Materials Science Division, Lawrence Berkeley National Laboratory, Berkeley, CA 94720, USA

\*lwmartin@berkeley.edu

## Supporting Information

### I. X-ray Diffraction

Rocking curve studies about the 002<sub>PC</sub> and 002 diffraction conditions of the film and substrate were used to examine the crystal quality of the heterostructures (Supporting Information, Fig. S1). In all cases, the full width, half maximum (FWHM) of the films is between ~2-5 times that of the substrate indicating comparable crystal quality.

Asymmetric reciprocal space maps (RMS) about the 0 $\bar{1}$ 3<sub>PC</sub>- (Fig. S1), 203<sub>PC</sub>-, and 0 $\bar{2}$ 3<sub>PC</sub>- (Fig. S2) diffraction conditions of both the films and substrate were performed in order to obtain information about the in-plane and out-of-plane lattice parameters of the heterostructures, the

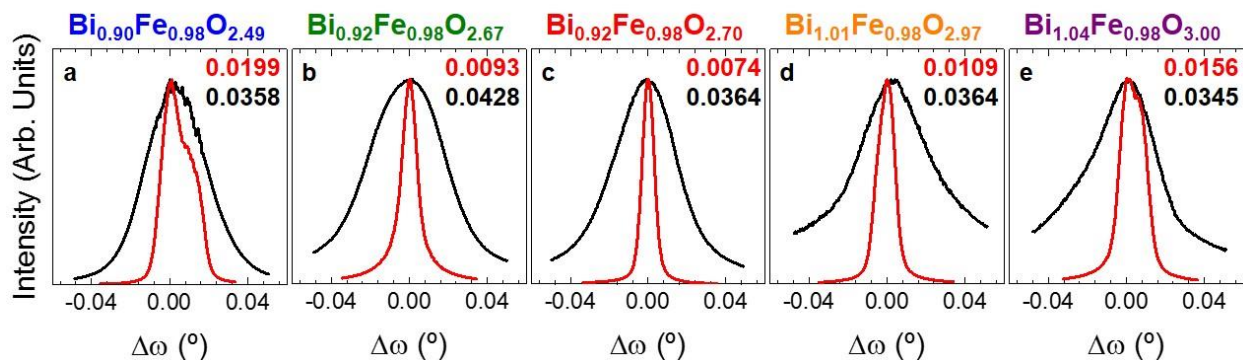


**Figure S1.** X-ray rocking curve studies about the 002<sub>PC</sub>-diffraction condition of the film and 220-diffraction condition of the substrate for the (a) Bi<sub>0.90</sub>Fe<sub>0.98</sub>O<sub>2.49</sub>, (b) Bi<sub>0.92</sub>Fe<sub>0.98</sub>O<sub>2.67</sub>, and (c) Bi<sub>0.92</sub>Fe<sub>0.98</sub>O<sub>2.70</sub>, (d) Bi<sub>1.01</sub>Fe<sub>0.98</sub>O<sub>2.97</sub>, and (e) Bi<sub>1.04</sub>Fe<sub>0.98</sub>O<sub>3.00</sub> heterostructures. The numbers in the upper right hand corner are the FWHM values from the substrate (top, red) and film (bottom, black) curves.

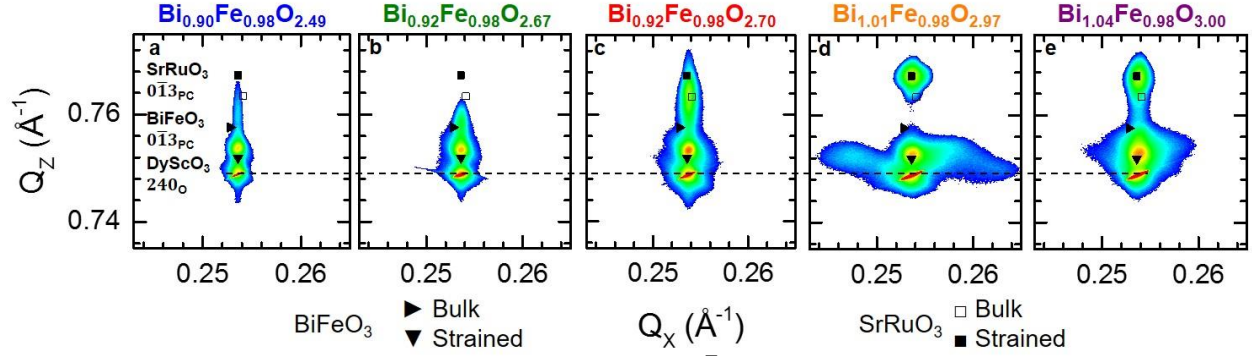


**Figure S2.** X-ray reciprocal space mapping studies about the  $0\bar{1}3_{PC}$ -diffraction condition of the film and bottom electrode and 240-diffraction condition of the substrate for the (a)  $\text{Bi}_{0.90}\text{Fe}_{0.98}\text{O}_{2.49}$ , (b)  $\text{Bi}_{0.92}\text{Fe}_{0.98}\text{O}_{2.67}$ , and (c)  $\text{Bi}_{0.92}\text{Fe}_{0.98}\text{O}_{2.70}$  heterostructures which all show bottom-electrode diffraction peaks that are shifted towards larger out-of-plane lattice parameter as well as data from (d)  $\text{Bi}_{1.01}\text{Fe}_{0.98}\text{O}_{2.97}$ , and (e)  $\text{Bi}_{1.04}\text{Fe}_{0.98}\text{O}_{3.00}$  heterostructures which show bottom electrodes that are coherently strained to the substrate. In all cases, the  $\text{BiFeO}_x$  films are all nearly coherently strained to the substrate.

strain state of both the  $\text{BiFeO}_3$  and  $\text{SrRuO}_3$ , and insight into the ferroelectric domain structure.

Looking first at the  $0\bar{1}3_{PC}$ - diffraction condition (Fig. S2), the  $\text{SrRuO}_3$  diffraction peak is highly shifted towards larger out-of-plane lattice parameters in the  $\text{Bi}_{0.90}\text{Fe}_{0.98}\text{O}_{2.49}$  (Fig. S2a),  $\text{Bi}_{0.92}\text{Fe}_{0.98}\text{O}_{2.67}$  (Fig. S2b), and  $\text{Bi}_{0.92}\text{Fe}_{0.98}\text{O}_{2.70}$  (Fig. S2c) heterostructures, but is located exactly where it is expected for a coherently strained film on a  $\text{DyScO}_3$  substrate in both the  $\text{Bi}_{1.01}\text{Fe}_{0.98}\text{O}_{2.97}$  (Fig. S2d) and  $\text{Bi}_{1.04}\text{Fe}_{0.98}\text{O}_{3.00}$  (Fig. S2e) heterostructures. Despite the large changes in  $\text{SrRuO}_3$  lattice parameter, all the  $\text{BiFeO}_3$  films are coherently strained to the substrate.

More detailed information pertaining to  $\text{BiFeO}_3$  lattice parameters and strain state can be obtained from the  $203_{PC}$ - and  $0\bar{2}3_{PC}$ -diffraction conditions (Fig. S3) due to the increased separation of the film and substrate diffraction peaks. Again, all heterostructures exhibit coherently strained  $\text{BiFeO}_3$ . Doublet splitting in both the  $203_{PC}$ - and  $0\bar{2}3_{PC}$ -diffraction conditions confirms the presence of  $71^\circ$  ferroelectric domains in the  $\text{Bi}_{0.90}\text{Fe}_{0.98}\text{O}_{2.49}$  (Fig. S3a,f),  $\text{Bi}_{0.92}\text{Fe}_{0.98}\text{O}_{2.67}$  (Fig. S3b,g), and  $\text{Bi}_{0.92}\text{Fe}_{0.98}\text{O}_{2.70}$  (Fig. S3c,h) heterostructures, whereas triplet splitting in the  $\text{Bi}_{1.01}\text{Fe}_{0.98}\text{O}_{2.97}$  (Fig. S3d,i) and  $\text{Bi}_{1.04}\text{Fe}_{0.98}\text{O}_{3.00}$  (Fig. S3e,j) heterostructures confirms the presence of both  $71^\circ$  and minority  $109^\circ$  domains.

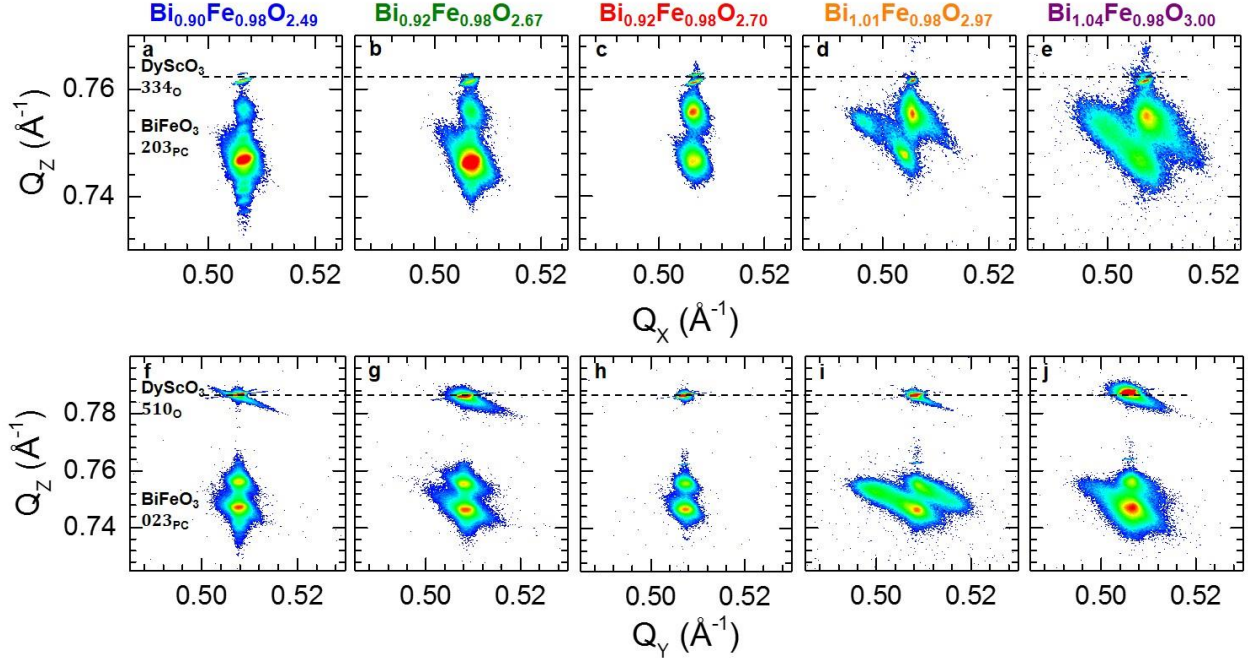


**Figure S3.** X-ray reciprocal space mapping studies about the (a-e) 203<sub>PC</sub>-diffraction condition of the films and 334-diffraction condition of the substrate and about the (f-j) 023<sub>PC</sub>-diffraction condition of the film and 510-diffraction condition of the substrate for (a),(f) Bi<sub>0.90</sub>Fe<sub>0.98</sub>O<sub>2.49</sub>, (b),(g) Bi<sub>0.92</sub>Fe<sub>0.98</sub>O<sub>2.67</sub>, and (c),(h) Bi<sub>0.92</sub>Fe<sub>0.98</sub>O<sub>2.70</sub> heterostructures which all show film peak splitting consistent with 71° ferroelectric domains, and for (d),(i) Bi<sub>1.01</sub>Fe<sub>0.98</sub>O<sub>2.97</sub> and (e),(j) Bi<sub>1.04</sub>Fe<sub>0.98</sub>O<sub>3.00</sub> heterostructures which all show film peak splitting consistent with majority 71° ferroelectric domains and minority 109° domains.

## II. n-type Conduction

Test devices of BiFeO<sub>3</sub> were grown directly on 0.5% Nb:SrTiO<sub>3</sub> in order to determine the majority carrier type. Current-voltage measurements (Fig. S3a) exhibit Ohmic conduction confirmed by  $\frac{d(\ln(J))}{d(\ln(V))} = 1$  (inset, Fig. S4a) in the negative bias regime and Schottky conduction in the positive bias regime. Such a trend in leakage current is expected from n-type BiFeO<sub>3</sub>, where the BiFeO<sub>3</sub>/Nb:SrTiO<sub>3</sub> interface is Ohmic in nature due to the small work function of Nb:SrTiO<sub>3</sub>, and the BiFeO<sub>3</sub>/SrRuO<sub>3</sub> interface is a Schottky junction. A schematic band diagram is also provided (Fig. S4b).

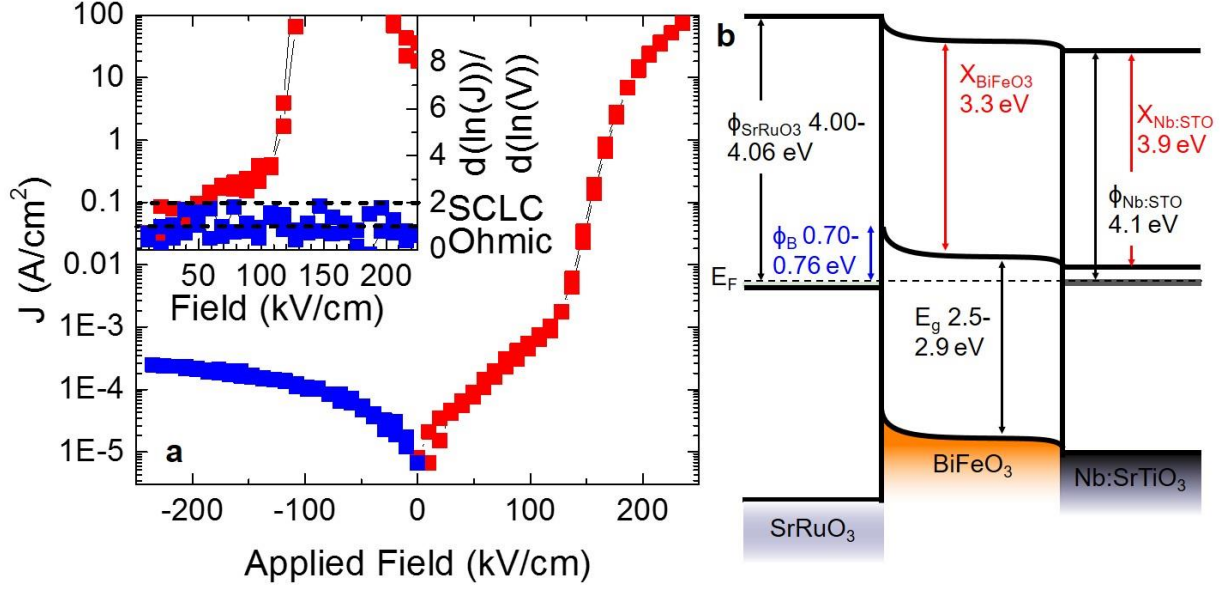


**Figure S4.** (a) Leakage response of, for example, a stoichiometric  $\text{Bi}_{0.92}\text{Fe}_{0.98}\text{O}_{2.77}$  heterostructure with 6%  $\nabla[\text{Bi}]$  and 5%  $\nabla[\text{O}]$  grown on 0.5% Nb:SrTiO<sub>3</sub> which exhibits Ohmic conduction ( $\frac{d(\ln(J))}{d(\ln(V))} = 1$ , inset) in the negative bias regime, indicating n-type conduction as per (b) the predicted band diagram for this system.

### III. Conduction Mechanism Fitting

The first potential conduction mechanism to be considered was Schottky emission which is characteristic of an interface-limited conduction due to the difference in Fermi level of the SrRuO<sub>3</sub> electrode and the BiFeO<sub>3</sub> film. Under Schottky emission, the current density is characterized by<sup>1</sup>

$$J = AT^2 \exp \left[ -\frac{\varphi_S}{k_B T} + \frac{1}{k_B T} \left( \frac{q^3 E}{4\pi \epsilon_0 K} \right)^{\frac{1}{2}} \right]$$

where  $A$  is the Richardson constant,  $\varphi_S$  is the Schottky barrier height,  $K$  the dielectric constant of BiFeO<sub>3</sub>, and  $E$  the electric field across the device. This equation can be rearranged to more simply evaluate whether current-voltage behavior is dictated by Schottky emission. From a semilog plot

of  $\frac{J}{T^2}$  vs.  $E^{\frac{1}{2}}$ , the slope is

$$m = \frac{1}{k_B T} \left( \frac{q^3}{4\pi\epsilon_0 K} \right)^{\frac{1}{2}}$$

and calculated values of  $K$  can be obtained through rearrangement and subsequently compared to literature values.

The second potential conduction mechanism that was considered was Poole-Frenkel emission which is characteristic of bulk-limited conduction from ionized trap states. Under Poole-Frenkel emission, the current density is characterized by<sup>2</sup>

$$\sigma = c \exp \left[ -\frac{E_I}{k_B T} + \frac{1}{k_B T} \left( \frac{q^3 E}{\pi\epsilon_0 K} \right)^{\frac{1}{2}} \right]$$

where  $c$  is a constant and  $E_I$  is the ionization energy of the trap state. Again, rearranging this equation allows for the evaluation of Poole-Frenkel emission as a viable conduction mechanism.

From a semilog plot of  $\sigma$  vs.  $E^{\frac{1}{2}}$ , the slope is

$$m = \frac{1}{k_B T} \left( \frac{q^3}{4\pi\epsilon_0 K} \right)^{\frac{1}{2}}$$

and, as before, calculated values of  $K$  can be compared to literature values.

The third potential conduction mechanism to be considered was the so-called modified Poole-Frenkel emission, wherein classical Poole-Frenkel emission discussed immediately prior must be modified in order to account for a non-trivial concentration of donor and/or acceptor states in the semiconducting material. Under modified Poole-Frenkel emission, the current density is characterized by<sup>3,4</sup>

$$\sigma = c \exp \left[ -\frac{E_I}{r k_B T} + \frac{1}{r k_B T} \left( \frac{q^3 E}{\pi\epsilon_0 K} \right)^{\frac{1}{2}} \right]$$

where variables are as defined for Poole-Frenkel emission, and  $r$  is a degree of compensation ranging from 1, corresponding to solely classical Poole-Frenkel emission, to 2, corresponding to fully modified Poole-Frenkel emission. Modified Poole-Frenkel emission can be distinguished from classical Poole-Frenkel emission by comparing the calculated values of  $K$  found in the limiting cases of classical Poole-Frenkel emission

$$m = \frac{1}{k_B T} \left( \frac{q^3}{\pi \epsilon_0 K} \right)^{\frac{1}{2}}$$

and the case of fully modified Poole-Frenkel emission

$$m = \frac{1}{2k_B T} \left( \frac{q^3}{\pi \epsilon_0 K} \right)^{\frac{1}{2}}$$

against literature values.

The final potential mechanism to be considered was space charge limited conduction which is characteristic of bulk-limited conduction of injected space charge. Under space charge limited conduction, the current density is characterized by<sup>5,6</sup>

$$J = \frac{9\mu\epsilon_0 K}{8d} E^2$$

where  $\mu$  is the carrier mobility. Space charge limited conduction can be evaluated by comparing the derivative of  $J$  vs.  $E$  with the expected value of 2. Such analysis is provided (Fig. S5), where it is

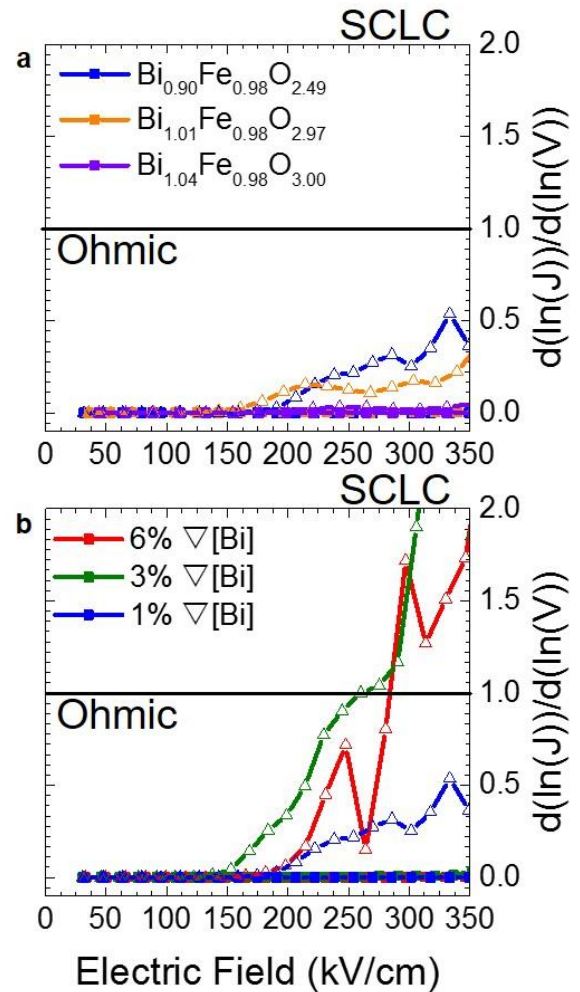


**Figure S5.** Derivatives of  $J$  versus  $V$  for (a)  $\text{Bi}_{0.90}\text{Fe}_{0.98}\text{O}_{2.49}$ ,  $\text{Bi}_{1.01}\text{Fe}_{0.98}\text{O}_{2.97}$ , and  $\text{Bi}_{1.04}\text{Fe}_{0.98}\text{O}_{3.00}$ , and (b)  $\text{Bi}_{0.90}\text{Fe}_{0.98}\text{O}_{2.49}$ ,  $\text{Bi}_{0.92}\text{Fe}_{0.98}\text{O}_{2.67}$ , and  $\text{Bi}_{0.92}\text{Fe}_{0.98}\text{O}_{2.70}$ . Neither set of variants exhibits Ohmic conduction ( $\frac{d(\ln(J))}{d(\ln(E))} = 1$ ) or space charge limited conduction (SCLC) ( $\frac{d(\ln(J))}{d(\ln(E))} = 2$ ).

seen that none of the heterostructure variants exhibit  $\frac{d(\ln(J))}{d(\ln(E))} = 2$ , thus ruling out space charge limited conduction as a potential conduction mechanism in these heterostructures.

## References

- (1) Schottky, W. Halbleitertheorie Der Sperrschicht. *Naturwissenschaften* **1938**, 26 (52), 843–843.
- (2) Frenkel, J. On Pre-Breakdown Phenomena in Insulators and Electronic Semi-Conductors. *Phys. Rev.* **1938**, 54 (8), 647.
- (3) Simmons, J. G. Poole-Frenkel Effect and Schottky Effect in Metal-Insulator-Metal Systems. *Phys. Rev.* **1967**, 155 (3), 657–660.
- (4) Yeargan, J. R.; Taylor, H. L. The Poole-Frenkel Effect with Compensation Present. *J Appl Phys* **1968**, 39 (12), 5600–5604.
- (5) Mott, N. F.; Gurney, R. W. Electronic Processes in Ionic Crystals. **1940**.
- (6) Lampert, M. A.; Mark, P. Current Injection in Solids. **1970**.